Sputtered Titanium Nitride: A Bifunctional Material for Li-Ion Microbatteries

Jeremy Freixas, Étienne Eustache, Pascal Roussel, Charlene Brillard, D. Deresmes, Nicolas Nuns, Nathalie Rolland, Thierry Brousse, C. Lethien

▶ **To cite this version:**

Jeremy Freixas, Étienne Eustache, Pascal Roussel, Charlene Brillard, D. Deresmes, et al.. Sputtered Titanium Nitride: A Bifunctional Material for Li-Ion Microbatteries. Journal of The Electrochemical Society, 2015, 162 (4), pp.A493-A500. 10.1149/2.0051504jes . hal-01725993

HAL Id: hal-01725993
https://hal.science/hal-01725993v1

Submitted on 17 Nov 2022

HAL is a multi-disciplinary open access archive for the deposit and dissemination of scientific research documents, whether they are published or not. The documents may come from teaching and research institutions in France or abroad, or from public or private research centers.

L'archive ouverte pluridisciplinaire **HAL**, est destinée au dépôt et à la diffusion de documents scientifiques de niveau recherche, publiés ou non, émanant des établissements d'enseignement et de recherche français ou étrangers, des laboratoires publics ou privés.

Distributed under a Creative Commons Attribution - NonCommercial 4.0 International License

Sputtered Titanium Nitride: A Bifunctional Material for Li-Ion Microbatteries

Jeremy Freixas,[a,b] Etienne Eustache,[a,b,c,d] Pascal Roussel,[e] Charlene Brillard,[a] Dominique Deresmes,[a] Nicolas Nuns,[e] Nathalie Rolland,[a,b,d] Thierry Brousse,[c,d,*,z] and Christophe Lethien[a,b,d,*,z]

[a]*Institut d'Electronique, de Microélectronique et de Nanotechnologie (IEMN), CNRS UMR 8520, Université de Lille 1 Sciences et Technologies, Laboratoire Central Cité Scientifique, 59652 Villeneuve d'Ascq Cedex, France*
[b]*Institut de Recherche sur les Composants logiciels et matériels pour l'Information et la Communication Avancée (IRCICA), CNRS USR 3380, Université Lille 1 Sciences et Technologies, Parc Scientifique de la Haute Borne, 59658 Villeneuve d'Ascq Cedex, France*
[c]*Institut des Matériaux de Nantes Jean Rouxel (IMN JR), CNRS UMR 6502, Université de Nantes, 44322 Nantes Cedex 3, France*
[d]*Réseau sur le Stockage Electrochimique de l'Energie, CNRS RS2E FR 3459, F-80039 Amiens Cedex, France*
[e]*Unité de Catalyse et de Chimie du Solide (UCCS), CNRS UMR 8181, Université Lille 1 Sciences et Technologies, 59655 Villeneuve d'Ascq Cedex, France*

Sputtered TiN bifunctional thin films have been deposited in order to act simultaneously as a current collector for the negative electrode and as a lithium ion diffusion barrier in a Li-ion microbattery fabricated on a silicon wafer. Sputtered parameters have been optimized to reach a dense and columnar morphology with no void and low surface roughness. For the films deposited at 450°C, the TiN resistivity is close to 105 μohm · cm. The normalized surface capacity of the optimized thin film (0.16 $\mu Ah/cm^2 \cdot \mu m^{-1}$) is one order of magnitude lower than the lowest reported capacities for TiN thin films (either by sputtering technique or by atomic layer deposition). The role of TiN thin film as lithium ion diffusion barrier has been evidenced by performing galvanostatic charge/discharge and concomitant depth profile analyses of a sputtered gold negative electrode deposited on a silicon wafer with and without the use of a TiN interlayer.

Wireless sensors, emerging technologies for medical implants, structural health monitoring or air quality analysis, suffer from a lack of miniaturized energy storage devices since the size of sensors is now getting close to the size of a microsystem. Power sources should then be integrated in such devices and lithium or lithium ion microbatteries seem to be good candidates for long term applications. The small footprint area of this energy storage devices and the compatibility with microelectronic facilities are the main reasons that should lead to industrial transfer toward pilot line production.

Classically, a thin film lithium or lithium-ion microbattery consists of silicon wafer on the top of which several functional layers such as a current collectors, a negative electrode and a positive electrodes separated by a solid electrolyte are sequentially deposited. It is often necessary in such devices to prevent lithium diffusion from the active layers through the silicon substrate. Subsequently a diffusion barrier must be integrated in the structure. Indeed, at low potential (vs Li/Li^+), silicon is known to electrochemically alloy with lithium at room temperature, leading to high gravimetric capacity (i.e. $Li_{15}Si_4$: 3580 mAh/g). Such impressive capacity is unfortunately correlated to large volume expansion ($\times$ 300 %),[1] thus inducing mechanical stress inside the material. This often translates in cracks and mechanical failures of the silicon substrate.[2] Thus the mechanical integrity of the negative electrode in contact with the silicon wafer is not preserved if this electrode is directly deposited on the top of the wafer. In order to prevent such irreversible damage which could lead to the delamination of the films and a quick and sudden failure of the microbattery, a lithium diffusion barrier layer has to be deposited (by chemical or physical vapor deposition techniques, hereafter CVD or PVD, respectively). For instance, silicon nitride (Si_3N_4) has been used as diffusion barrier layer in the fabrication process of a CMOS compatible lithium microbattery.[3] In that case, as Si_3N_4 is an insulator, an additional deposition step is then required in order to achieve implement of the current collector function usually with metals such as Pt, Au, W or Ti, etc. (depending on the potential of the material negative electrodes). Only few results dealing with the use of lithium diffusion barrier layer are available in the literature, either for planar or 3D Li-ion microbattery. Notten *et al.*[4–6] have reported the successful use of transition metal nitrides for this purpose. More specifically, the authors report the use of titanium and tantalum nitrides thin films. TiN is already well characterized for mechanical, electrical and optical properties but only few studies are focused on the investigation of its electrochemical behavior. Notten's group has compared[4–6] the ability of sputtered and atomic layer deposited (ALD) TiN thin films to prevent lithium diffusion from the negative electrode to the silicon substrate. Concerning the sputtered deposited lithium diffusion barrier, very promising results issued from electrochemical measurement were reported[4,6] clearly demonstrating the proof of concept. In the proposed studies, Ta, TaN and TiN thin films are compared as possible lithium diffusion barriers, but without in-depth investigation of the role of deposition parameters.[4–6] Since the proposed TiN thin film can act simultaneously as diffusion barrier and current collector for the negative electrode, its electrical behavior is a main concern. In,[4,6] electrical characterization has only been performed on ALD deposited films(resistivity $\sim$150 $\mu\Omega \cdot$ cm), but not on sputtered ones.

Recently, a TiN layer has been integrated in a combined energy harvesting and storage autonomous system in order to prevent the lithium ion diffusion from the battery to the silicon substrate of the photovoltaic (PV) cell.[7] In such dual device, the PV cell and the lithium ion microbattery were both integrating silicon nanowires electrodes. Reactive sputtering deposition was performed using a pure metallic Titanium target under reactive Ar/N_2 atmosphere in order to grow the TiN diffusion barrier. Finally, the cyclability of a silicon nanowires-based electrode was improved by depositing a TiN interlayer between the silicon substrate and the nanowires.[8]

In the present work, an in-depth study of sputtered titanium nitride, acting both as lithium diffusion barrier and as current collector, has been performed in order to evaluate the usefulness of such barrier in a lithium ion microbattery. The evolution of the thin films microstructure regarding the deposition conditions is reported. Sputtering pressure, substrate temperature, sputtering time (film thickness) and power deposition parameters have been tuned in order to achieve TiN thin films with low resistivity and low electrochemical activity vs lithium ion insertion. A low capacity TiN thin film deposited by sputtering deposition within the framework of this study seems to combine in a more efficient way high electrical

*Electrochemical Society Active Member.
[z]E-mail: thierrry.brousse@univ-nantes.fr; christophe.lethien@iemn.univ-lille1.fr

conductivity and low electrochemical capacity compared to previously reported data on sputtered TiN layer and ALD deposited TiN barrier.[4–6]

Experimental

Thin film deposition.— The titanium nitride (TiN) thin films were deposited on high resistivity silicon wafers (>10 Mohm · cm) allowing the electrical characterization of the films without any influence from the substrate. TiN deposition was performed by direct current (DC) magnetron sputtering deposition facility in a DP 650s equipment (Alliance concept) starting from a TiN target (99,999% purity, 4 inch diameter) under argon atmosphere. Homogeneous deposits were obtained by keeping the distance between the target and the substrate at 70 mm. Several parameters of the deposition process have been tuned in order to optimize both the efficiency of TiN as a lithium diffusion barrier and as a good current collector. Deposition pressure (0.001 up to 0.01 mbar), deposition time (100 s up to 450 s), substrate temperature (room temperature up to 550°C), argon flow rate (10 up to 100 sccm), and DC power (0.71 W/cm^2 up to 1.23 W/cm^2) have been investigated. The gold thin films have been deposited by DC sputtering of a 4-inch pure gold target on planar silicon substrates. The same DP 650s sputtering equipment has been used to achieve the thin film deposition at 10^{-2} mbar after pumping to a base vacuum of 10^{-7} mbar. The forward power was kept at 150 W in an argon atmosphere (Ar).

Thin film characterization.— The morphology of the sputtered thin films has been observed with a scanning electron microscope (ZEISS ULTRA 55 – for cross section analyses) as well as with an atomic force microscopy AFM Dimension 3100 for surface analyses. The thickness was determined both with a surface profilometer (Dektak II a) and with a scanning electron microscope. XRD measurements were performed using a Rigaku Smartlab equipment equipped with a copper rotated anode ($\lambda = 1.54056$ Å). The TiN mass was measured by weighting the silicon wafer before and after deposition of the different thin films, using a Mettler Toledo XP6U high performance microbalance (accuracy 0.1 µg). XPS measurements (Kratos Ultra Axis spectrometer) have been performed to evaluate the stoichiometry of the TiN films. Time of Flight Secondary Ion Mass Spectrometry (TOF-SIMS - Ion TOF 5 GmbH Germany) has been carried out to evaluate the depth profile of chemical elements in the deposited thin films in order to highlight the lithium diffusion within the cross section of the film when electrochemical measurements were carried out.

Electrical investigations (resistivity mapping) were achieved with a SEMILAB WT 2000 PVN contactless equipment. Electrochemical measurements, such as cyclic voltammetry (CV) and galvanostatic cycling with potential limitation (GCPL) were performed using a Biologic SP300 potentiostat/galvanostat in a GP concept Argon-filled glove box. The TiN layers deposited by DC magnetron sputtering on a silicon wafer were tested as working electrode using a Teflon like homemade flat cell (tested area: 0.785 cm^2). Pure lithium foils were used as counter and reference electrodes. The liquid electrolyte, was LiTFSI (1 M) dissolved in EC/DEC (1/1) (Sigma Aldrich Inc, 99% purity).

Results and Discussion

Morphology and electrical measurements of the TiN thin films.— The morphology of the TiN thin films deposited at room temperature was first studied. The thickness of the analyzed layers is estimated by SEM and profilometry to be close to 0.18 µm (deposition time ∼350 s). The surface analyses carried out by AFM are reported in Fig. 1a and 1b with varying deposition conditions. From these measurement (surface analysis ∼1 µm^2), it is clear that the roughness is really low (root mean square roughness – RMS – between 1.3 and 4.3 nm) whatever the depositions conditions are. Nevertheless, some trends could be identified: i) the argon flow rate does not change the roughness of the TiN; ii) low DC power leads to very low roughness.

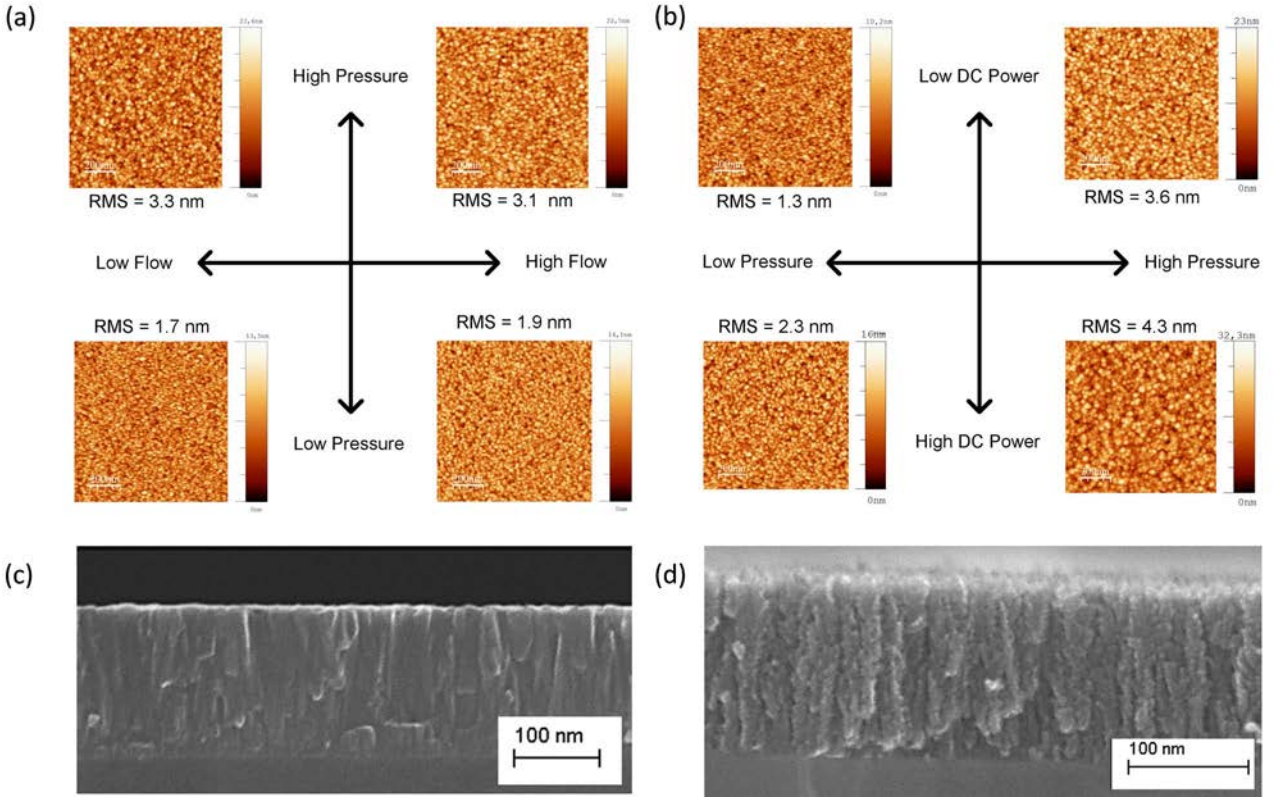

Figure 1. Surface ((a) and (b)) and cross sections analyses ((c) and (d)) of TiN thin films deposited with different conditions. The columnar and dense TiN film deposited at low pressure is depicted in Fig. 1c. A deposition at high pressure reveals a porous TiN layer as shown in Fig. 1d.

It is well known that pressure is a crucial parameter for the growth of thin film. In the present case, the surface analysis indicates that TiN films deposited at low pressure exhibit small grain morphology, and that high pressure deposition increases the RMS roughness. Therefore, the TiN layer is dense at low pressure while a porous morphology is obtained at high pressure, as depicted in the cross section observations (Fig. 1c and 1d). According to the Thornton model[9,10] four regions illustrating the microstructure's evolution of sputtered thin films are highlighted. This structure zone model (SZM) has been extended recently by Mahieu et al.[11–13] up to 5 zones (extended SZM – ESZM) and only to one parameter dependence: the mobility of adsorbed atoms (hereafter *adatoms*) linked to all the deposition parameters. At low deposition temperature and high pressure, the thin films' microstructure is porous and composed of needles or columns separated by defects or voids that could deeply influence both the electrical and electrochemical behaviors. In this growth mode, the *adatoms* surface mobility is low, inducing then stick on the surface resulting in a porous morphology of the as-deposited material. By decreasing the deposition pressure and increasing the temperature, the porosity, linked to the empty space between the columns, progressively disappears and the thin film density increases. At high temperature (around 500°C), a dense and columnar microstructure (zone 1c or T of the E-SZM)[13] with large grains is obtained owing to the material crystallization: the *adatoms* mobility is relatively high in this zone which facilitates the *adatoms* surface diffusion. The SEM images (cross section) of two samples, depicted in Fig. 1c and 1d, both deposited at RT but at two different pressures clearly follow the (E)-SZM models proposed by Thornton and Mahieu (needle/porous in Zone I and columnar/dense in Zone T). The 2nd zone has never been reached whatever the deposition conditions.

The electrical conductivity of the RT TiN samples is reported in Fig. 2. The argon flow rate does not significantly change the TiN resistivity till the argon flow rate threshold is reached (∼40 sccm) – Fig. 2a). As predicted, the TiN samples deposited at high pressure (Fig. 2a and 2b) and low DC power (Fig. 2b) exhibit a high resistivity probably due to the porous structure of the layer (presence of voids between needles or columns). Moreover, as in Refs. 14 and 15 the increase of the resistivity observed for our films can be related to Ti/N ratio different from 1, meaning that our films are probably under or over stoichiometric depending on the deposition parameters (see discussion on XRD patterns).Indeed, by tuning the deposition pressure and DC power parameters, the resistivity is drastically reduced from 3 mohm · cm down to 160 µohm.cm in optimized conditions (deposition pressure = 10^{-3} mbar, DC power density = 1.23 W/cm^2, Ar flow rate = 100 sccm). In that study, the deposition time has been kept constant close to 350 s.

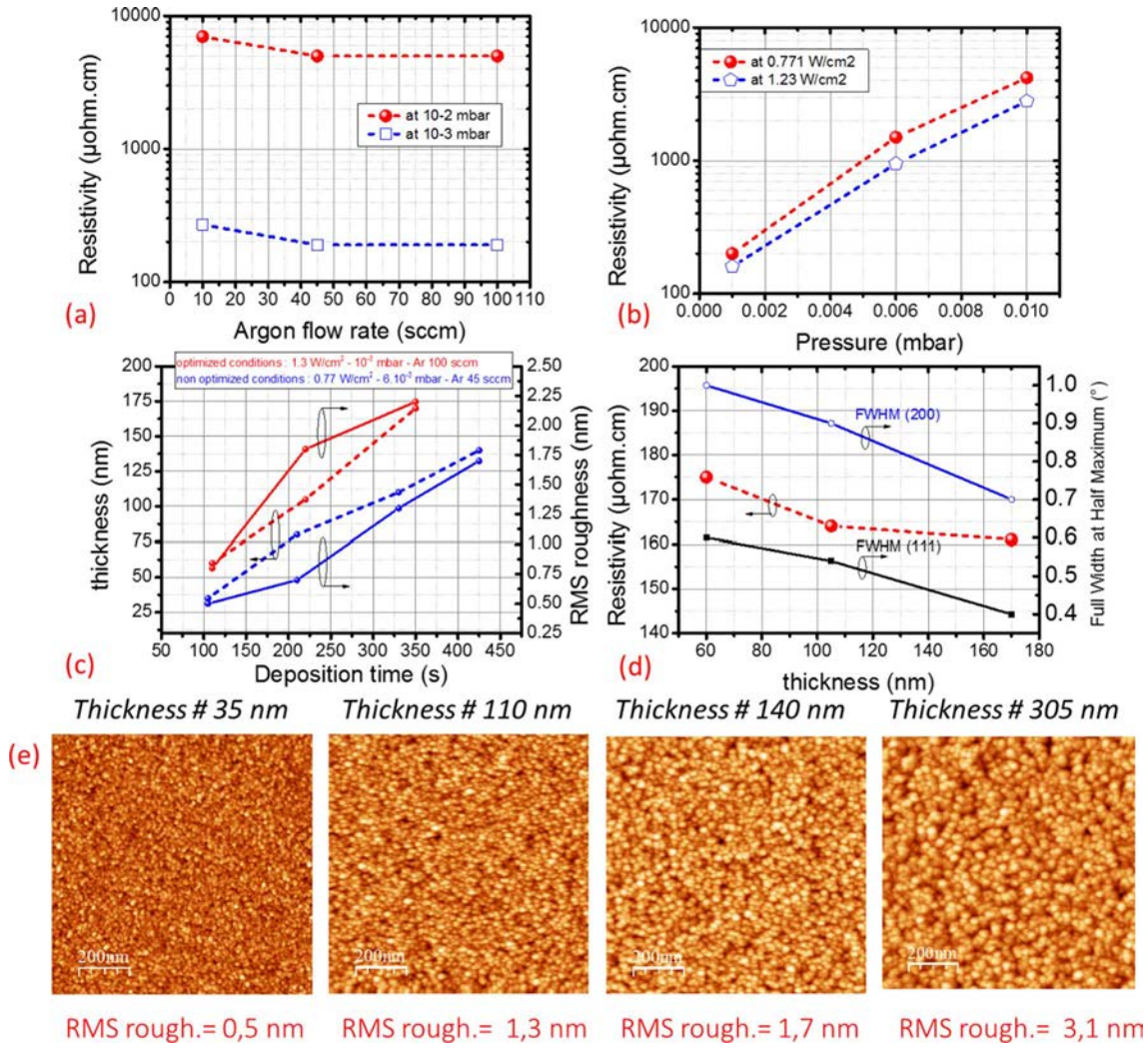

Figure 2. Resistivity measurements vs. the argon flow rate (a) and vs. the pressure (b) during the sputtering deposition. On the left graph, the DC power (0.771 W/cm^2) and the deposition time (350 s) are kept constant at the two tested pressures. The Fig. 2c reports the evolution of the film thickness and roughness vs the deposition time: 2 deposition conditions have been tested. The evolution of resistivity and the FWHM of the (200) and (111) diffraction peaks with film thickness are depicted in Fig. 2d. The top surface analysis of the TiN thin films vs the thickness is reported in Fig. 2e.

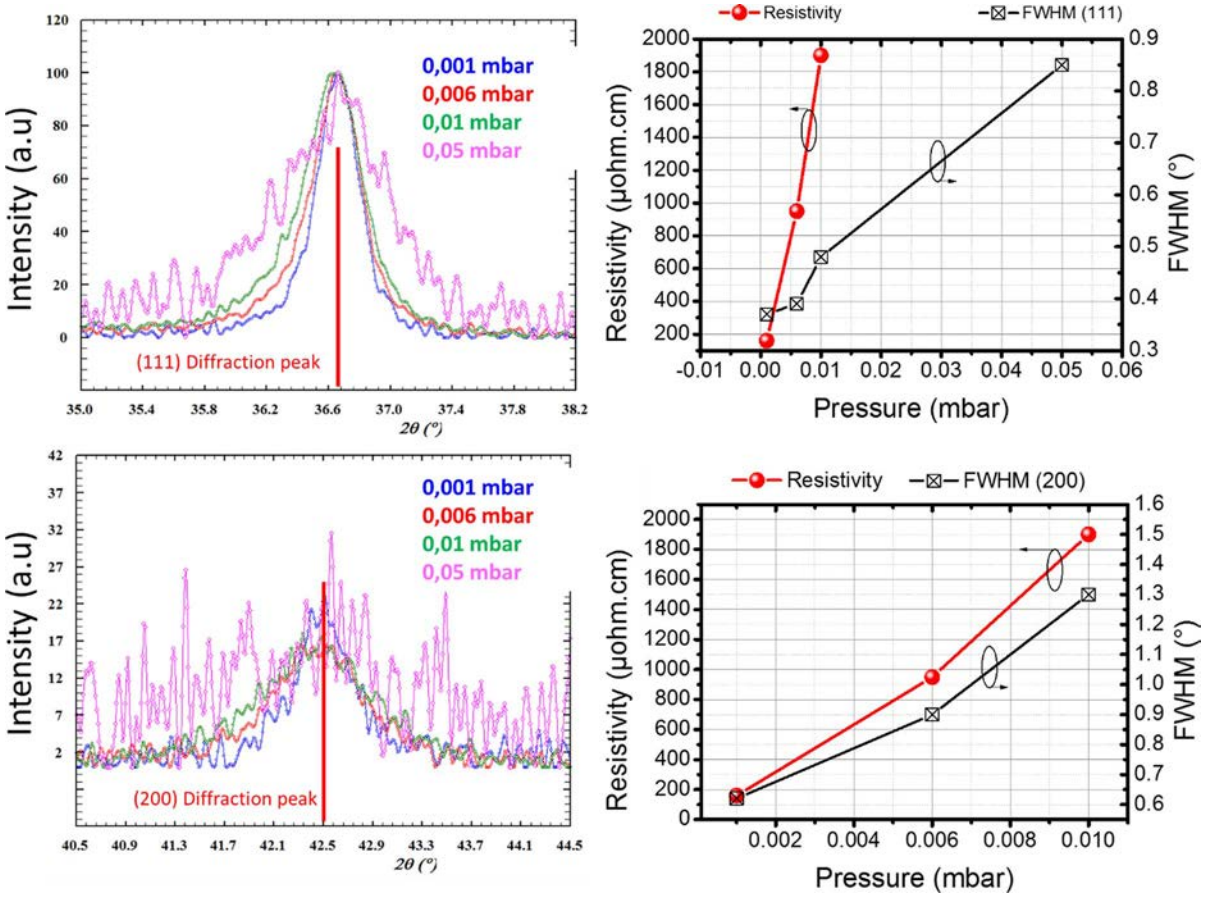

Figure 3. XRD analysis of the TiN deposited at room temperature vs. the deposition pressure (from 0.05 mbar (pink) down to 10^{-3} mbar (blue)). The FWHMs of the (111) and (200) diffraction peak decrease when the deposition is performed at low pressure. Concomitantly a decrease of the resistivity is observed.

The Fig. 2c reports the evolution of the TiN thickness and RMS roughness as a function of the deposition time. Not surprisingly, the thickness and the roughness proportionally increase with the deposition time whatever the deposition conditions are. From the XRD analyses of the TiN thin films at different thickness, no change of the preferential orientation has been found observed because the deposited layers exhibit a thickness below a critical threshold where a change of orientation is expected. The resistivity progressively steadily decreases from 175 down to 160 µohm.cm (Fig. 2d) when the TiN thickness increases, probably due to the grain growth occurring during the deposition. It has been confirmed by the decrease of the full widths at half maximum (FWHM) of the (200) and (111) diffraction peaks on the TiN corresponding diffractograms (Fig. 2d). The evolution of the RMS roughness as a function of the deposition time is reported in Fig. 2e: the grain growth is clearly highlighted on these top surface analyses (similar scale between the 5 micrographs).The titanium nitride deposited by DC sputtering is known to be a biaxially textured[12] thin film with two preferential orientations linked to a grain growth along the [200] and [111] directions. From the XRD patterns reported in Fig. 3, a significant decrease of the full width at half maximum (FWHM) of the (111) and (200) diffraction peaks is observed when the deposition pressure decreases from $5 \cdot 10^{-2}$ mbar down to 10^{-3} mbar, thus indicating that grain growth occurs when the pressure is reduced, i.e. with a lower number of defects, and consequently a reduced resistivity.

The deposition temperature is also a crucial key parameter for improving the structural, electrical and electrochemical properties of the titanium nitride thin films. Several tests were undertaken to verify this assumption. First of all, the RMS roughness of TiN thin films deposited from RT up to 550°C (similar thickness180 nm – deposition time 350 s) was evaluated (Fig. 4): a decrease of this RMS roughness (from 2.2 nm down to 1.5 nm) is highlighted when the deposition temperature reaches 550°C.

Surface and cross section observations of the 450°C TiN sample are depicted in Fig. 5. A columnar and dense microstructure with low roughness is demonstrated for this sample (180 nm thick).

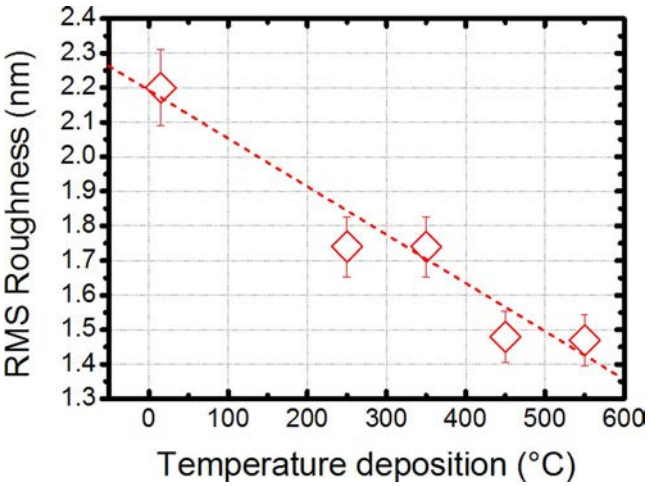

Figure 4. Evolution of the RMS roughness with the deposition temperature. Surface analyses are reported (1 µm x 1 µm).

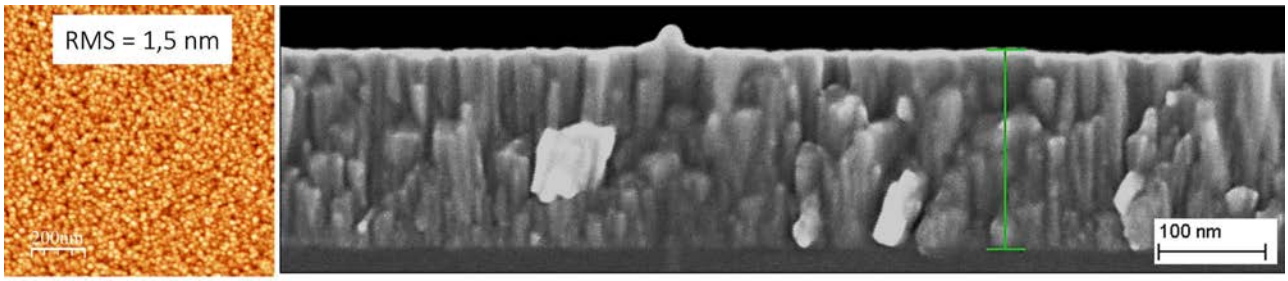

Figure 5. Morphology of the TiN thin film deposited at 450°C.

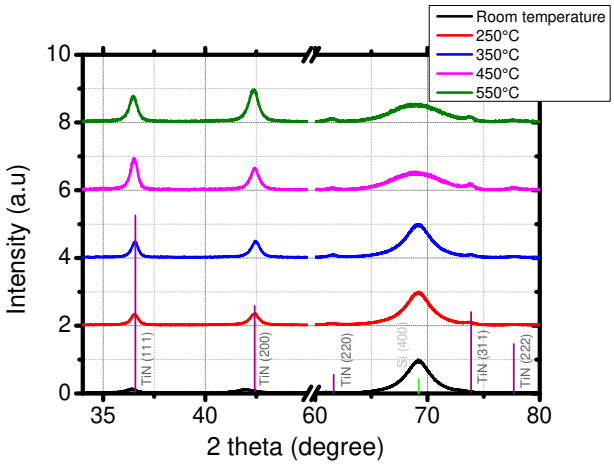

Figure 6. XRD patterns of TiN thin films deposited from RT up to 550°C.

The XRD patterns recorded for different deposition temperature of TiN films (taking into account of the optimized conditions developed at RT) are depicted in Fig. 6 in order to check the texture of the TiN. The two mains diffraction peaks centered at $2\theta = 36.6°$ and $2\theta = 42.4°$ can be attributed respectively to the (111) and (200) diffraction planes of titanium nitride mineral form Osbornite (JCPDS 00-038-1420). A slight (200) preferential orientation is observed for the samples deposited at 250°C, 350°C and 450°C but a change occurs for the sample deposited 550°C which exhibits a (111) orientation. The full widths at half maximum (FWHM) of the (111) and (200) peaks decrease till the deposition temperature reaches 450°C, thus evidencing a growth of the crystallite with the temperature. For the sample deposited at room temperature, the FWHM of the different peaks is the highest of the series. This is probably related to smaller crystallite which probably affects the electrical properties. For the other films, prepared at higher temperatures, since the growth of the crystallite is correlated with a decrease of the electrical resistivity of the TiN thin films (see Table I), this structural property appeared as one of the key parameters for the preparation of sputtered layers.

During the sputtering deposition process, the deposition temperature seems to be a key parameter to reduce the number of defects in the TiN thin film due to a rearrangement of the crystal structure (texture / preferential orientation) directly linked to higher *adatoms* surface diffusion mobility.

Apart from the film deposited at RT which exhibit a cell parameter (4.26(9) Å) well above that of δ-TiN,[16] the other samples (up to 450°C) exhibit the same cell parameter (4.25(6) Å) which is in good agreement with the values reported for TiN thin films with a slight understoechiometric ratio ($TiN_{0.96}$). For the film deposited at 550°C, the cell parameter increases again which must be correlated with the presence of oxygen in this sample.

The resistivity mapping is illustrated in Fig. 7 (scanning length: 1.4 cm): the resistivity (summarized in Table I) decreases from 160 µohm.cm (measured at RT) down to 105 µohm.com (TiN deposited at 450°C) due to the grain growth and the change of preferential orientation of the thin film regarding the operating deposition temperature. Since the cell parameter and thus the stoechiometry of the samples deposited between 250°C and 450°C is the same, it seems more sensible to assign the decrease in resistivity for the thin film deposited at 450°c to grain growth and to better crystallization of the film rather than to the Ti/N ratio.

The sample obtained at 550°C exhibits a higher resistivity (185 µohm.cm), presumably not only because of a change[11] in the preferential orientation from (200) to (111) but also due to the partial oxidation of the TiN at this temperature. Indeed, the increase in cell parameter can be related to partial incorporation of oxygen in the lattice. This partial oxidation of the TiN layer leads to the progressive formation of the TiO_2 rutile polymorph when the deposition temperature is higher than 500°C. This oxidation process has been highlighted by in situ high temperature X-ray diffraction (HT-XRD between RT up to 900°C under N_2 atmosphere) analyses (not shown in the paper) performed on an optimized TiN thin film deposited at RT.

Electrochemical characterization of the TiN thin films.— At this point, the TiN current collector is optimized from an electrical point of view with a low resistivity (close to 105 µohm · cm). The next step is to evaluate the electrochemical properties of the optimized TiN in order to determine which TiN film exhibits the lowest surface capacity. Cyclic voltammetry (CV) between 0.01 V and 1.5 V vs Li/Li^+ is reported in Fig. 8 for the RT TiN sample (1 mV/s – EC/DEC/1 M LiTFSI liquid electrolyte). No redox peaks are identified on this CV. Indeed, the nearly rectangular shape CV suggests that only the double layer capacitance of the TiN is measured. This lack of redox processes between TiN and lithium ions support the use of this

Table I. Evolution of the FWHM and the preferential orientation of the TiN sputtered thin films with the deposition temperature.

	Cubic cell parameter (Å)	FWHM (111)	FWHM (200)	Resistivity (µOhm · cm)	Preferential orientation
RT	4.26(9)	0.75	1.14	160	–
250°C	4.25(6)	0.53	0.65	125	(200)
350°C	4.25(6)	0.49	0.67	125	(200)
450°C	4.25(6)	0.48	0.64	105	(200)
550°C	4.26(5)	0.59	0.73	185	(111)

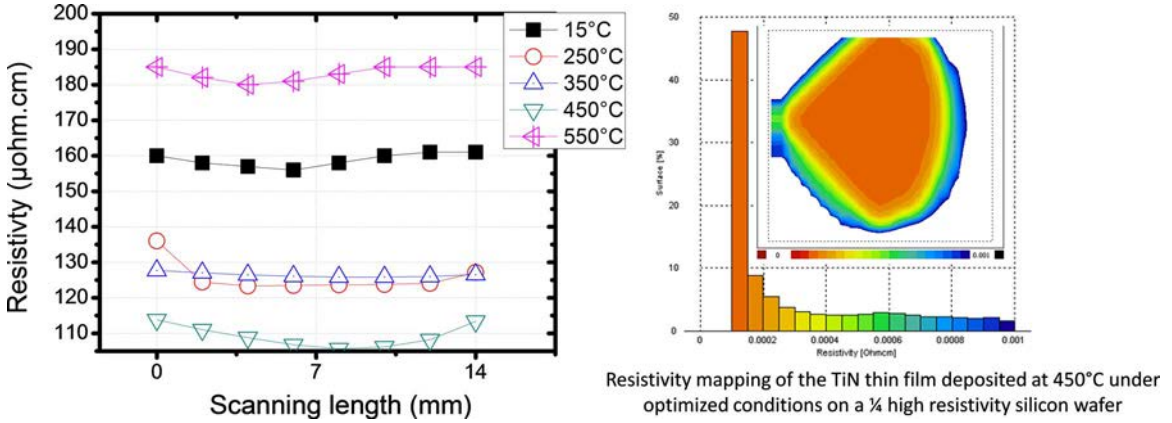

Figure 7. resistivity mapping of the TiN thin films with the deposition temperature.

material as a good lithium diffusion barrier. Such behavior has also been observed by P. Notten et al.[4–6] Similar measurements have been performed with sputtered TiN having a porous morphology and the CV shape clearly shows a significant increase of the lithium ion / TiN reactivity. In order to determine the lowest surface capacity of such thin films (lowest reactivity vs. lithium) and to evaluate the cyclability of TiN films, galvanostatic charge/discharge (GCPL) measurements were performed (Fig. 8). Samples deposited from RT up to 550°C are investigated. 2 current densities have been applied between 0.01 V and 1.5 V vs Li/Li^+. Not surprisingly, the surface capacity of TiN is higher at lower current density (1.3 $\mu A/cm^2$) for all the tested samples. After stabilization, the surface capacity of the RT sample reaches a capacity close to 0.2 $\mu Ah/cm^2$. At higher current density (3.2 $\mu A/cm^2$), this value decreases down to 0.07 $\mu Ah/cm^2$. When the deposition temperature is increased up to 550°C, the surface capacity of the corresponding TiN thin film is drastically reduced down to 0.02 $\mu Ah/cm^2$. Regarding the thickness of the TiN layer (0.18 μm), the normalized surface capacity of the low electrochemically active TiN reaches 0.11 $\mu Ah/cm^2 \cdot \mu m^{-1}$. The lowest areal capacity of sputtered TiN deposited[4] by the Notten's group is 4.28 $\mu Ah/cm^2 \cdot \mu m^{-1}$ with similar current density. TiN films deposited by the same research group by ALD[6] exhibits a capacity close to 2.85 $\mu Ah/cm^2 \cdot \mu m^{-1}$ which is higher than the values reported in the present paper.

Interestingly, the values of double layer capacitance of the different TiN samples determined from CVs and galvanostatic plots are in the range 40–400 $\mu F/cm^2$. These values are in good agreement with reported values for different metal nitrides thin films in organic based electrolytes.[17] They depict a capacitive behavior at the TiN/electrolyte interface which in turn suggests a negligible reactivity of TiN with lithium in this potential window.

Fig. 9 summarizes the surface capacity of the optimized TiN samples. The resistivity of the TiN samples is also indicated. TiN

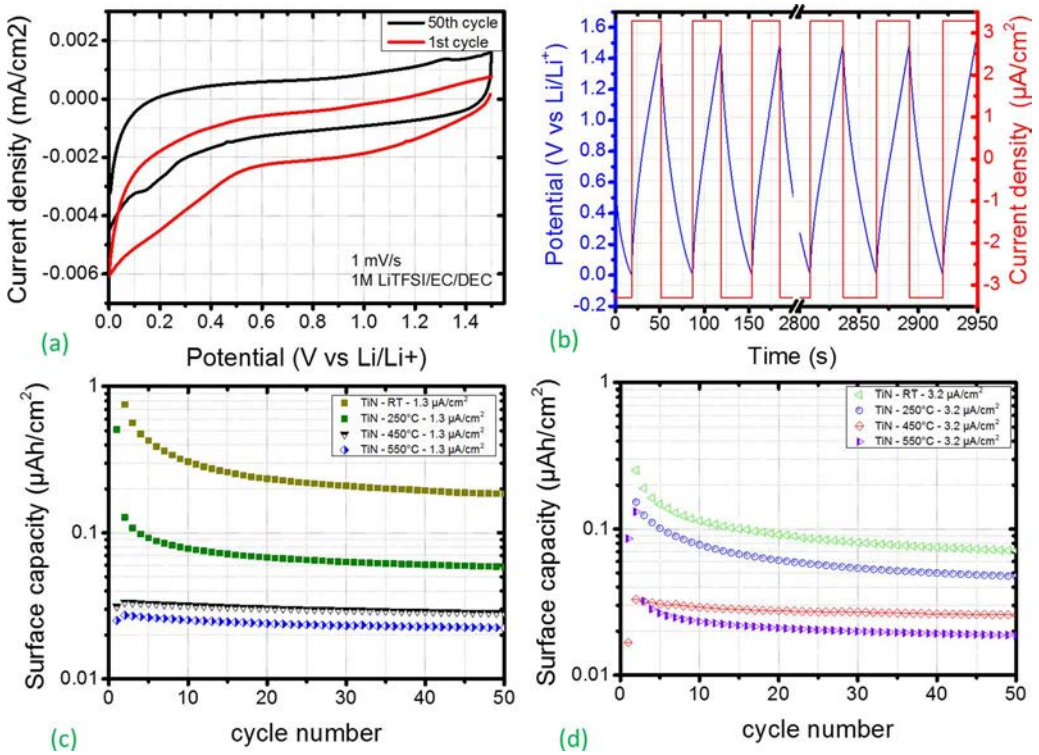

Figure 8. Electrochemical characterization of the optimized TiN films: (a) cyclic voltammetry (first and last cycles (scan rate: 1 mV/s) in 1M LiTFSi in EC/DEC (1/1)) of the RT sample. (b) Galvanostatic plots performed at 3.5 $\mu A/cm^2$ between 0.01 V and 1.5 V vs Li/Li^+ of the TiN film deposited at 450°C. (c) and (d) Surface capacity of all the samples (determined from the GCPL measurement) at two different current densities (electrolyte: 1 M LiTFSI in EC/DEC (1/1)).

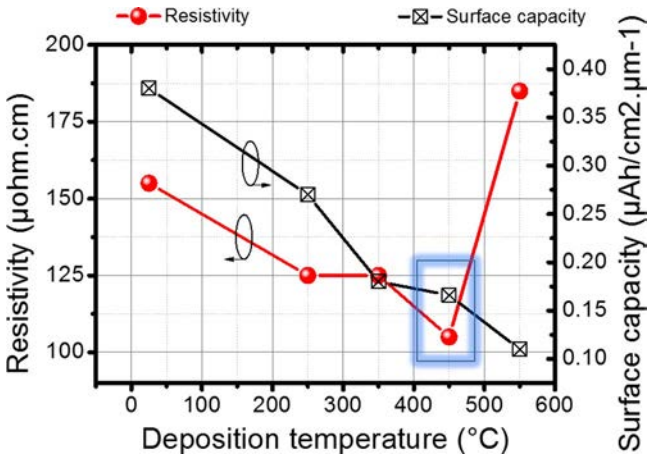

Figure 9. Resistivity and surface capacity measurements of the TiN thin film acting as a current collector and a lithium diffusion barrier.

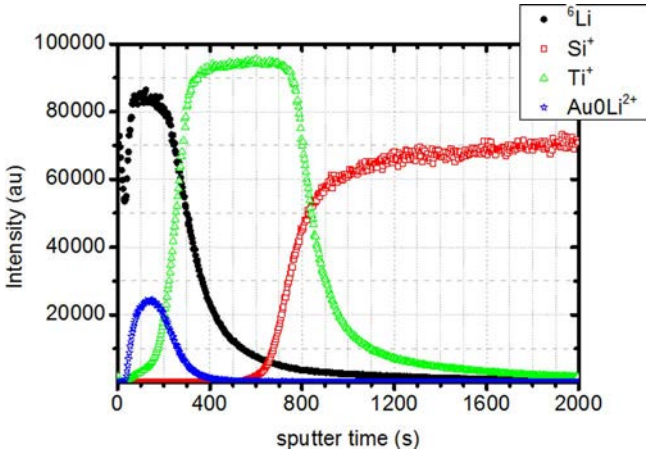

Figure 11. Depth profile (cross section) determined from TOF SIMS analysis of the Au/TiN/Si structure after electrochemical tests (see Fig. 10).

deposited at 450°C seems to be the best trade-off between resistivity and reactivity vs. lithium ion: it should act as a good current collector and diffusion barrier. To demonstrate the potential of this TiN film deposited at 450°C, the electrochemical behavior of a thin film negative electrode (thickness: 120 nm) deposited on a silicon substrate by DC sputtering was studied. Gold was chosen as a negative electrode because of its strong ability to electrochemically alloy with lithium at room temperature:[18] depending on the voltage plateaus, several Li_xAu_y alloys are expected.[19,20] Two samples (SEM cross section depicted in Fig. 10) have been electrochemically tested on a homemade flat cell using the GCPL technique at C/16 between 0.01 V and 1.5 V vs Li/Li^+. The first sample is just a gold thin film directly deposited on the top of a silicon wafer. Within this potential window, silicon is known to alloy with lithium (at room temperature, the lithium rich alloy $Li_{15}Si_4$ could be formed). Lithium ions first react with the gold layer but the lower cutoff potential (0.01 V vs Li/Li^+) is never reached (Fig. 10). This means that lithium ion are continuously reacting with the silicon substrate below the gold layer, leading to large volume expansion and subsequent delamination of the electrode. In the second sample, a lithium diffusion barrier based on TiN (thickness: 170 nm) (selected deposition parameters: pressure $= 10^{-3}$ mbar, temperature = 450°C, Ar flow rate = 100 sccm, DC power = 1.23 W/cm^2, time = 350 s) is deposited between the silicon substrate and the gold negative electrode. The lower cutoff potential is reached quickly and the shape of the galvanostatic plot is close to literature data.[18] In addition, no delamination of the gold electrode is observed. Further results obtained with the sputtered gold electrodes will be reported soon.

Thus the use of TiN interlayer between the silicon substrate and the gold negative electrode allows to obtain good cycling performances at C/16. The TOF-SIMS analysis (Figure 11) performed on the second sample illustrate without any doubt the good performance of the TiN layer as a diffusion barrier as lithium is only detected in the gold thin film, without any traces in the silicon substrate.

Conclusions

In this study, sputtered Titanium Nitride (TiN) has been optimized to act simultaneously as a Bifunctional material achieving i) low resistivity in order to be used as a current collector and ii) low electrochemical activity vs. lithium in order to be used as a diffusion barrier against lithium ion to protect the silicon substrate. With our sputtering techniques, TiN thin film deposited at 450°C exhibit the best morphology to reach these targets: a dense and columnar morphology (low deposition pressure). The film resistivity is close to 105 µohm.cm combined with a normalized surface capacity of 0.16 µAh/cm^2 · µm^{-1}. These performance are interesting compared to already published data.[4–6] Depth profile analysis of the post cycled Au electrode deposited on silicon substrate with a TiN diffusion barrier in between reveals the presence of lithium only in the gold negative electrode which fulfill the requirements for the development of lithium ion microbatteries on silicon substrate.

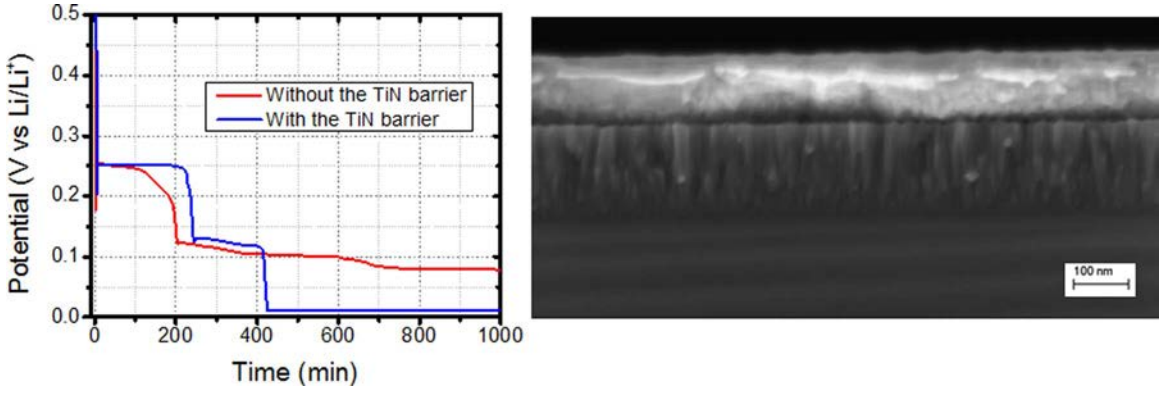

Figure 10. Left: Constant current charge-discharge cycles (1st discharge cycle) of two gold electrodes. The measurement have been performed with and without the lithium diffusion barrier deposited in this study (TiN) in liquid electrolyte between 0.01 V and 1.5 V vs Li/Li^+. Right: SEM cross section of the TiN/Au (2nd sample) stacking sputtered on silicon substrate.

Acknowledgments

The authors want to thank the French network of electrochemical energy storage (RS2E) for the PhD grant of E.E. This research is also financially supported by French ANR and DGA within the framework of the MECANANO project (ANR-12-ASTR-0032-01). The French RENATECH network and the CPER CIA are greatly acknowledged.

References

1. L. Y. Beaulieu, T. D. Hatchard, A. Bonakdarpour, M. D. Fleischauer, and J. R. Dahn, *Journal of the Electrochemical Society*, **150**, A1457 (2003).
2. J. Li and J. R. Dahn, *Journal of the Electrochemical Society*, **154**, A156 (2007).
3. S. Oukassi, X. Gagnard, R. Salot, S. Bancel, and J. P. Pereira-Ramos, Above Ic Micro-Power Generators for RF-Mems, in *DTIP of MEMS and MOEMS*, Stresa, Italy (2006).
4. L. Baggetto, R. A. H. Niessen, F. Roozeboom, and P. H. L. Notten, *Advanced Functional Materials*, **18**, 1057 (2008).
5. H. C. M. Knoops, L. Baggetto, E. Langereis, M. C. M. van de Sanden, J. H. Klootwijk, F. Roozeboom, R. A. H. Niessen, P. H. L. Notten, and W. M. M. Kessels, *Journal of the Electrochemical Society*, **155**, G287 (2008).
6. L. Baggetto, J. F. M. Oudenhoven, T. van Dongen, J. H. Klootwijk, M. Mulder, R. A. H. Niessen, M. H. J. M. de Croon, and P. H. L. Notten, *Journal of Power Sources*, **189**, 402 (2009).
7. V. Chakrapani, F. Rusli, M. A. Filler, and P. A. Kohl, *Journal of Power Sources*, **216**, 84 (2012).
8. E. L. Memarzadeh, W. P. Kalisvaart, A. Kohandehghan, B. Zahiri, C. M. B. Holt, and D. Mitlin, *Journal of Materials Chemistry*, **22**, 6655 (2012).
9. J. A. Thornton, *Journal of Vacuum Science and Technology*, **11**, 666 (1974).
10. J. A. Thornton, *Journal of Vacuum Science & Technology A: Vacuum, Surfaces, and Films*, **4**, 3059 (1986).
11. S. Mahieu, P. Ghekiere, G. De Winter, S. Heirwegh, D. Depla, R. De Gryse, O. I. Lebedev, and G. Van Tendeloo, *Journal of Crystal Growth*, **279**, 100 (2005).
12. S. Mahieu, P. Ghekiere, G. De Winter, R. De Gryse, D. Depla, G. Van Tendeloo, and O. I. Lebedev, *Surface and Coatings Technology*, **200**, 2764 (2006).
13. S. Mahieu, P. Ghekiere, D. Depla, and R. De Gryse, *Thin Solid Films*, **515**, 1229 (2006).
14. N. Arshi, J. Lu, Y. K. Joo, C. G. Lee, J. H. Yoon, and F. Ahmed, *Journal of Materials Science: Materials in Electronics*, **24**, 1194 (2012).
15. M. Kawamura, Y. Abe, H. Yanagisawa, and K. Sasaki, *Thin Solid Films*, **287**, 115 (1996).
16. J.-E. Sundgren, B.-O. Johansson, S.-E. Karlsson, and H. T. G. Hentzell, *Thin Solid Films*, **105**, 367 (1983).
17. R. Lucio-Porto, S. Bouhtiyya, J. F. Pierson, A. Morel, F. Capon, P. Boulet, and T. Brousse, *Electrochimica Acta*, **141**, 203 (2014).
18. G. Taillades, N. Benjelloun, J. Sarradin, and M. Ribes, *Solid State Ionics* **152–153**, 119 (2002).
19. A. D. Pelton, *Bulletin of Alloy Phase Diagrams* **7**, 228 (1986).
20. T. L. Kulova, A. M. Skundin, V. M. Kozhevin, D. A. Yavsin, and S. A. Gurevich, *Russian Journal of Electrochemistry*, **46**, 877 (2010).